

Broadband and wide-angle beam deflection enabled by dynamically reconfigurable meta-arrays

KOFFI-EMMANUEL SADZI AND ABDOU LAYE NDAO*

University of California, San Diego, Department of Electrical and Computer Engineering, La Jolla, California, United States

*a1ndao@ucsd.edu

Compiled October 21, 2025

We present a structurally simple yet functionally versatile reflective meta-array composed of phase-change Antimony trisulfide (Sb_2S_3) nanorods enabling broadband and wide-angle beam deflection in near-infrared. The device achieves over 80% deflection efficiency over a 1000 nm wide passband, and covering from O-band (1260 nm-1360 nm) to U-band (1565 nm-1625 nm) in the *amorphous* state. Meanwhile, in its *crystalline* state, we see a reduction of the efficiency to 40% on average with a maximum passband of 800 nm over the C-band. Moreover, its simple architecture simultaneously enables spectral filtering and beam splitting, delivering a compact, multifunctional solution optimized for high power applications.

<http://dx.doi.org/10.1364/ao.XX.XXXXXX>

1. INTRODUCTION

Controlling the propagation of light is fundamental to optical science and technology. In that regard, an increase in interest in wavefront engineering has led to diverse approaches [1–3], away from the traditional methods relying on bulky components like lenses and prisms, which are shaped according to Snell’s law. Two of such approaches, anomalous reflection and its counterpart, anomalous refraction, have become a fundamental tool in modern optics, finding applications in optical communications [4], laser systems [5], and pulse compression technologies [6–8]. Anomalous reflection, often referred to as deflection, describes the unusual steering of incident electromagnetic waves with a non-specular angle, namely, towards a direction not predicted by Snell’s law. Deflection typically relies on directing most of the incident wave energy into a non-zero diffraction order by design. Therefore, high deflection efficiency, combined with wide angular and broadband operation, is highly desirable.

To satisfy the stringent demands of modern optical systems, a wide range of grating-based strategies have been investigated. These include binary blazed gratings [9, 10], multi-ridge complex gratings [11], and structures incorporating artificial materials [12]—particularly effective in the near-infrared and visible spec-

tral regions. Alternative approaches have employed photonic crystal gratings (PhCGs) [13, 14], which exploit Bloch mode dispersion for tailored light manipulation.

Recently, ultrathin optical interfaces composed of subwavelength nanostructures named metasurfaces [15–22] have rapidly emerged as a disruptive technology in flat optics. By offering unprecedented control over the phase, amplitude, and polarization of light at the nanoscale [23–27], they enable functionalities far beyond those of conventional bulk optics. This paradigm shift has led to the demonstration of a broad spectrum of devices, including metasurface deflectors [28–31].

In the context of high-power applications, a desired additional functionality is variable efficiency or power-limited features. Few existing designs [32–38] offer built-in power-limiting capabilities; however, they do not integrate broadband, wide-angle, and spatial filtering.

In this work, we propose and numerically demonstrate a simple periodic meta-array composed of Sb_2S_3 nanorods, which enables wide-angle, wideband anomalous reflection. The design naturally incorporates additional features, such as spatial filtering and beam splitting, without requiring extra tuning parameters. The same device can be reconfigured for high power applications exploiting the absorption of the crystalline- Sb_2S_3 . This approach opens new avenues for the realization of compact, high-power-compatible optical elements, well-suited for integrated photonics and sophisticated wavefront control.

2. RESULTS AND DISCUSSION

Our reflective meta-array consists of rectangular nanorods made of Antimony trisulfide Sb_2S_3 , a phase-change material (PCM) [39]. The PCM has two phases: *crystalline*, which is lossy (see Supplement 1 for details), and low-loss *amorphous* in the bandwidth of interest (O-U band). This prominent material enables the designed device to achieve an ultra-wideband and wide-angle wave deflections as well as a configurability to accommodate high powers applications. Namely, under high power continuous-wave or pulsed lasers, the switching property of the PCM allows a passive transition from the amorphous to crystalline state for a continuous-wave source when the temperature in the PCM reaches its transition temperature (refer to Supplement 1 for details on switching mechanism and threshold). In principle, the incident wave is reflected using the $n = -1$ diffraction order in the case of transverse electric (TE) polarization, where the electric field vector of the incident wave is

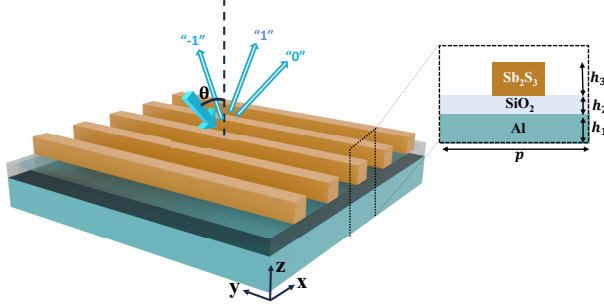


Fig. 1. Schematic of the proposed device: θ represents the incident angle; the reflected beam includes the 0th and -1st diffraction orders, along with other deflected components such as 1st order illustrated here. (right) Cross-section of a unit cell of the meta-array: $p = 1150$ nm represents the period of the unit cell, $w = 300$ nm denotes the width of the nanorod, and $h_1 = 100$ nm, $h_2 = 60$ nm, $h_3 = 200$ nm represent the heights of the Al layer, of the SiO₂ layer and the Sb₂S₃ nanorod, respectively

parallel to the axes of the nanorods.

Figure 1 represents the schematic of our proposed structure, as well a cross-section. The structure contains a periodic array of rectangular Sb₂S₃ nanorods, patterned on the top of SiO₂ buffer layer deposited on the Aluminum (Al) layer. p , w denote the period of the unit cell, the width of each nanorod, respectively; h_1 , h_2 , h_3 are the thicknesses of the Aluminum layer, of the Silicon Oxide layer, and the PCM nanorod, respectively. To operate in reflection mode, we use $h_1 = 100$ nm and while optimizing for the difference in the efficiency of deflection at *amorphous* and *crystalline* state, as well as a steep cutoff near O- and U- band, the designed geometrical parameters are: $p = 1150$ nm, $w = 300$ nm, $h_1 = 100$ nm, $h_2 = 60$ nm, $h_3 = 200$ nm. Those values are selected to ensure robustness of the design, anticipating even significant fabrication imperfections.

Owing to the fundamental impact of loss on system performance, the efficiency of the n th order deflection ($\eta_{(n)}$) of the device is evaluated as a ratio of the power converted to the n th order to the total incident power. Considering an incident wave, with wavelength λ , on a grating structure of period p and at an incidence angle θ , the angle ϕ_n of the reflected waves following the diffraction orders (n) are given by the well-known relation [40]:

$$\sin \phi_n = \sin \theta + n \lambda / p \quad (1)$$

A given order n is reflected or propagates when $|\sin \phi_n| < 1$. This supports that the 0th order is always reflected as a specular reflection. As achieved and shown below, when the structure support only -1 order as nonzero propagating mode, a high efficiency is observed both for the *crystalline* and *amorphous* phase of the nanorod.

To examine the performance of our design, we perform a full-wave simulation using Computer Simulation Technology (CST) software. Figure 2(a) compares, under TE polarization incidence wave, the deflection efficiency spectrum at the -1st order for

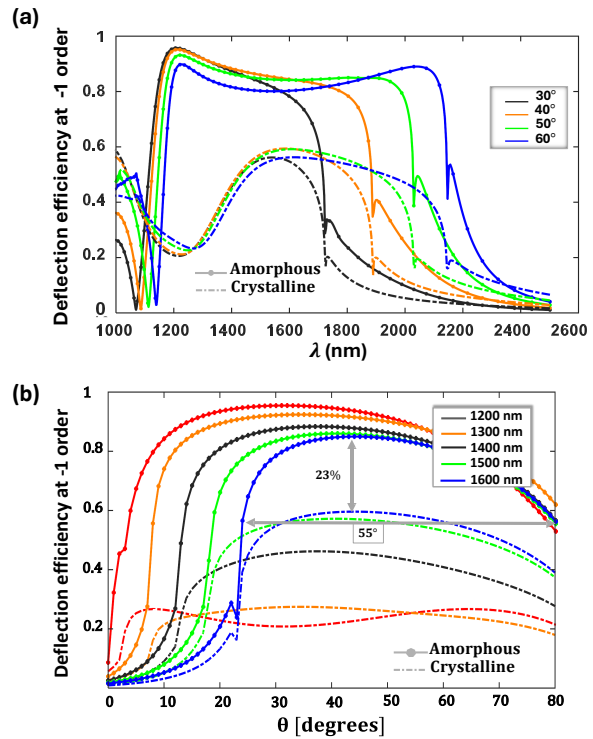


Fig. 2. Simulation results of the -1st order deflection efficiency, as a function of (a) the wavelength λ and (b) the incidence angle θ for both *amorphous* (in solid line with marker) and *crystalline* (dot-dash line) phases. TE polarization is considered. The wideband deflection achieved covers O-band to U-band in the case of the *amorphous* state (solid line) with efficiency greater than 80%. In the *crystalline* phase case, a deflection efficiency as low as 20% can be achieved (in O-band). (b) shows that despite the reduction of angle range with wavelength, a minimum of 55° is achieved with a difference of 23% between the *crystalline* and *amorphous* state.

the PCM in *crystalline* and *amorphous* states. In the *amorphous*, a passband of over 1000 nm wide can be achieved, with very sharp cutoffs at both short and long wavelengths. An efficiency of over 80% also characterizes the passband. Hence, this case shows a good performance as a spectral filter. In contrast, the *crystalline* case exhibits a gradual roll-off and can still achieve a passband of 800 nm, covering the entire U-band. It yields, as expected, a low efficiency, limiting the reflected power below 60% and as low as $\sim 20\%$. Hence, this case demonstrates the versatility of the device for power sensitive applications.

Moreover, to confirm the wide-angle deflection of the design, we analyze the efficiency versus the θ for fixed wavelengths. As shown in Fig. 2(b), the *amorphous* case maintained an efficiency $\eta_{(-1)}$ over a wide range of θ , spanning over 50° with the capability of a slight angle for short wavelengths. It enables also an angular passband with a sharp low- θ cutoff. Interestingly, the *crystalline* case maintains a low and nearly constant efficiency. One can also notice that around 45°, the difference in efficiency between the *amorphous* and *crystalline* cases increases with wavelength, between 0.23 (labeled on the figure) and 0.75 (obtained around 30°, for $\lambda = 1200$ nm). To protect Sb₂S₃ from oxidation, the device is capped with a SiO₂ layer of thickness t (see Supplementary Information for details). Sweeping the

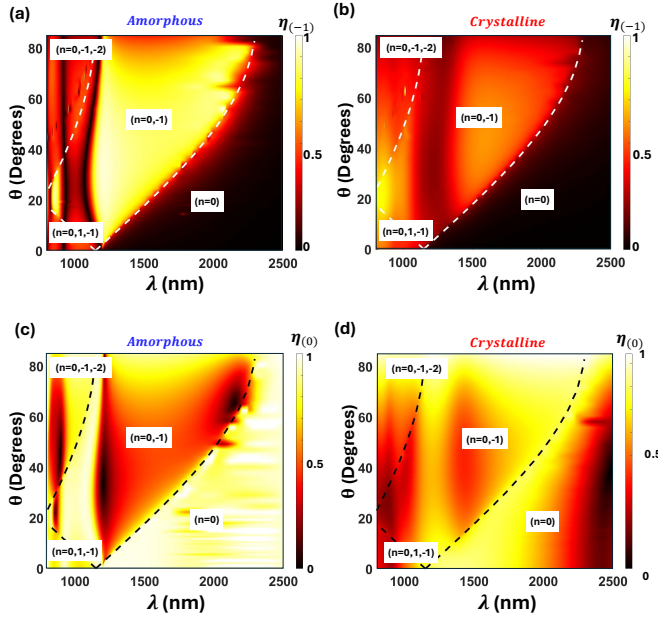


Fig. 3. Contour plot of the deflection efficiency, $\eta_{(n)}$, for $n = -1$ (a-b) and $n = 0$ (c-d) order as a function of both wavelength and the incidence angle. The PCM is *amorphous* in (a,c) and *crystalline* in (b,d) simulations. The region to the left of the dashed black lines constitutes the domain where the corresponding order ($n = -1, -2$ or $+1$) propagates.

capping thickness between 15 and 40 nm [41–44] shows that the device performance is largely unaffected, with the passband and deflection efficiency decreasing by less than 2.1% on average, highlighting the robustness of the design.

To further demonstrate the $\theta - \lambda$ range that our device enables in the presence of diffraction and to show the interplay of the diffraction modes, we present in Fig. 3 the contour plot of the efficiency of both the -1 st order and specular reflection over the (λ, θ) -plane. The dashed black lines in the subplots are obtained using Eq. (1) and upper-bound regions for a diffraction order n propagate. One can easily have a gauge of the loss mechanism present in the *crystalline* nanorods from the low efficiency obtained in Fig. 3 (c) vs (d) when only the 0-th order is reflected: in the first, there is total reflection while the latter presents region of almost no reflection (above $\lambda = 2 \mu\text{m}$).

From Fig. 3 (a) and (b), one notices that the efficiency $\eta_{(-1)}$ is non-zero only in regions where Eq. (1) dictates the propagation of the -1 st order, which implies that the deflection process is limited by diffraction. Nevertheless, there is an increase in the passband with the incidence angle. Notably, the *amorphous* case achieves significant efficiency only when the -1 st order is the only non-zero order. In contrast, in the *crystalline* case, despite the emergence of diffraction orders (-2 nd and $+1$ st), an efficiency of 50% is still achieved, at short wavelengths (below $\lambda = 1 \mu\text{m}$). Figure 3 (a,c) establish a complementary domain where the power is dominantly reflected either as -1 st order versus 0th order, for the PCM is *amorphous*. For its counterpart, the *crystalline* case, the loss in the material limits the power of both the 0th order and the -1 st order, while the former remains dominant. Since the 0th order or specular reflection is not nullified, even in the region where non-zero orders exist. This allows the device to be used as a power splitter as well.

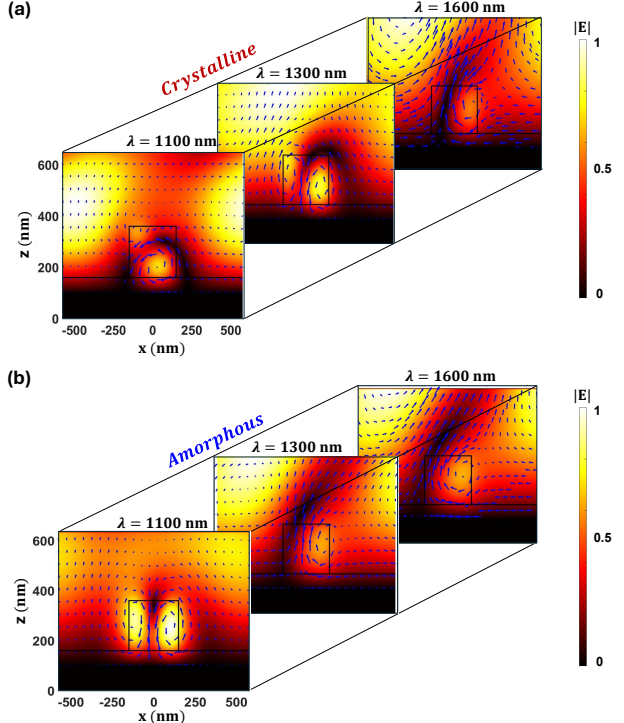


Fig. 4. Electric field (colormap) and Magnetic field (quiver plot) inside and near the nanorod for *crystalline* (a) and *amorphous* (b) case at $\lambda = 1100 \text{ nm}$, $\lambda = 1300 \text{ nm}$ and at $\lambda = 1600 \text{ nm}$; the TE polarization is considered, for an incident angle $\theta = 35^\circ$. The solid line (white) delimits the different layers of the structure.

To investigate the mode characteristics associated with the observed resonance, we plot the distribution of the electric field (E-field) under a TE incident wave, as shown in Fig. 4. The latter contrasts the E-field distribution around the nanorods in the *crystalline* case (a) and the *amorphous* case (b) for given wavelengths, and $\theta = 35^\circ$. At $\lambda = 1100 \text{ nm}$, the E-field is nearly symmetric and localized in the nanorod in *crystalline* case (Fig. 4(a)), as opposed to at its boundaries in *amorphous* case (Fig. 4(b)). In fact, in the *crystalline* case, the E-field distribution reveals the mode pattern as of zero-order Mie resonance of a circular rod [45, 46]. In contrast, in the *amorphous* case, the distribution is consistent with a magnetic dipole resonance, as explicitly demonstrated by the magnetic field distribution in Fig. 4(b). This is associated with a low efficiency (below 40%) in both cases. Moreover, at $\lambda = 1300 \text{ nm}$, in both material phases (Fig. 4), one notices a mode distribution similar to that of a tilted magnetic dipole with a weaker localization of the E-field inside the rod. The region of a weak electric field hosts a quasi-static magnetic field distribution that supports the excitation of a magnetic dipole. This region being greater in the *amorphous*-based structure yields, therefore, a larger equivalent magnetic dipole for greater efficiency. The tilted resonant magnetic dipole is also established at 1600 nm for both states. It shows a pronounced asymmetry in the field distribution, in agreement with the contrast between the H-field distribution at $\lambda = 1300 \text{ nm}$ and 1600 nm (Fig. 4(b)). We attribute the high efficiency of the -1 st deflection coefficient to the asymmetry of the fields established in the device, namely, the excitation of a tilted magnetic dipole. In light of the significant similarities in the field distributions at 1300 nm and 1600 nm for

the two states of the Sb_2S_3 , the difference in the -1 st deflection efficiency can undoubtedly be attributed to the loss mechanism inside the *crystalline* state.

Further, the functionalities offered by our design go beyond wide-angle and ultrawide-band deflection and power attenuation for high power application. For the *amorphous*-based structure, the design ensures a spatial filtering, as hinted earlier, as an advantage of the sharp cutoff (Fig. 2 (a,b)). From the existence of the bandpass with sharp cutoffs, our design demonstrates a frequency selectivity that characterizes spatial filtering [47]. Through spatial filtering, one can sort the incident waves and, as a result, modify the angular spectrum [48]. While the -1 st order provides reflection mainly at large angle θ (Fig. 2 b), the -2 nd order deflection from the nanorod structure results in a narrow band-pass-spatial filtering. Figure 5 shows that for a TE polarization, an angular bandwidth of $40^\circ - 60^\circ$ is obtained around $\lambda = 800$ nm.

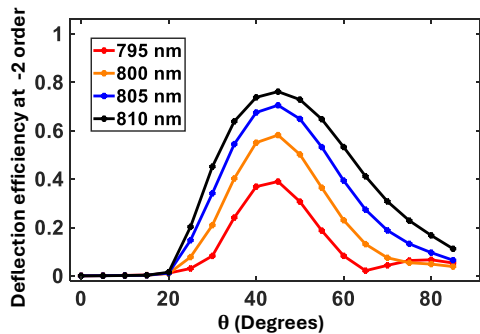


Fig. 5. Narrow band pass spatial filtering exploiting -2 nd order deflection in 795-810 nm, in TE polarization.

3. CONCLUSION

In summary, we have numerically demonstrated a highly efficient and multifunctional reflective meta-array based on Sb_2S_3 phase-change material nanorods operating in the near-infrared regime. The proposed design achieves ultra-wideband and wide-angle deflection in the *amorphous* state, with deflection efficiencies exceeding 80% over more than 1000 nm of bandwidth and incidence angles spanning up to 55° . While in the *crystalline* state, the inherent material loss enables effective optical power limiting, reducing the deflected power below 60%, with values as low as 20% in the O-band. Additionally, the device exhibits functionalities such as spectral filtering, wide-angle deflection, and partial power splitting, with complementary deflection and reflection characteristics.

The field distribution analysis further highlights the role of low-order Mie resonances and their evolution with wavelength and phase state, providing insights into the underlying physical mechanisms. Thanks to its simplicity, robust performance, and dynamic tunability, the proposed meta-array offers a promising platform for applications in optical power limiting, beam shaping, and integrated photonic systems, particularly for applications requiring broadband operation and high power resilience.

Disclosures. The authors declare no conflicts of interest.

Data availability. Data underlying the results presented in this paper are not publicly available at this time but may be obtained from the authors upon reasonable request.

REFERENCES

1. R. W. Wood, Phys. Rev. **48**, 928 (1935).
2. S. B. Glybovski, S. A. Tretyakov, P. A. Belov, *et al.*, Phys. Reports **634**, 1 (2016).
3. S. Liu, Z. Ma, J. Pei, *et al.*, Nanotechnol. Precis. Eng. **5**, 025001 (2022).
4. B. Rose, T. Rasmussen, and C. Khalfaoui, “Littrow configuration tunable external cavity diode laser with fixed direction output beam,” US Patent 6978062B2 (2005). Issued Dec. 20, 2005.
5. D. Strickland and G. Mourou, Opt. Commun. **56**, 219 (1985).
6. C. J. Hawthorn, K. P. Weber, and R. E. Scholten, Rev. Sci. Instruments **72**, 4477 (2001).
7. M. D. Perry and G. Mourou, Science **264**, 917 (1994).
8. J.-K. Rhee, T. S. Sosnowski, and T. B. Norris, Opt. Lett. **19**, 1550 (1994).
9. M. S. L. Lee, P. Lalanne, J. C. Rodier, and E. Cambril, Opt. Lett. **25**, 1690 (2000).
10. P. Lalanne, J. Opt. Soc. Am. A **16**, 2517 (1999).
11. K. Hehl, J. Bischoff, U. Mohaupt, *et al.*, Appl. Opt. **38**, 6257 (1999).
12. C. Sauvan, P. Lalanne, and M. S. L. Lee, Opt. Lett. **29**, 1593 (2004).
13. B. Gralak, S. Enoch, and G. Tayeb, J. Opt. Soc. Am. A **17**, 1012 (2000).
14. A. E. Serebryannikov, Phys. Rev. B **80**, 155117 (2009).
15. P. Lalanne, S. Astilean, P. Chavel, *et al.*, Opt. Lett. **23**, 1081 (1998).
16. Z. Bomzon, V. Kleiner, and E. Hasman, Opt. Lett. **26**, 1424 (2001).
17. F. Lu, F. G. Sedgwick, V. Karagodsky, *et al.*, Opt. Express **18**, 12606 (2010).
18. B. H. Fong, J. S. Colburn, J. J. Ottusch, *et al.*, IEEE Trans. on Antennas Propag. **58**, 3212 (2010).
19. N. Yu, P. Genevet, M. A. Kats, *et al.*, Science **334**, 333 (2011).
20. A. Ndaø, L. Hsu, J. Ha, *et al.*, Nat. Commun. **11**, 3205 (2020).
21. L. Hsu, M. Dupré, A. Ndaø, and B. Kanté, Opt. Lett. **42**, 1520 (2017).
22. A. Ndaø, L. Hsu, W. Cai, *et al.*, Nanophotonics **9**, 1081 (2020).
23. P. Genevet, F. Capasso, F. Aieta, *et al.*, Optica **4**, 139 (2017).
24. L. Hsu, M. Dupré, A. Ndaø, and B. Kanté, Opt. Lett. **42**, 1520 (2017).
25. G.-Y. Lee, G. Yoon, S.-Y. Lee, *et al.*, Nanoscale **10**, 4237 (2018).
26. G. Yang, A. V. Sergienko, and A. Ndaø, Opt. Express **29**, 18565 (2021).
27. G. Yang, A. V. Sergienko, and A. Ndaø, Opt. Lett. **47**, 629 (2022).
28. Y. F. Yu, A. Y. Zhu, R. Paniagua-Domínguez, *et al.*, Laser & Photonics Rev. **9**, 412 (2015).
29. M. I. Shalaev, J. Sun, A. Tsukernik, *et al.*, Nano Lett. **15**, 6261 (2015).
30. J. Ha, A. Ndaø, L. Hsu, *et al.*, Opt. Express **26**, 23178 (2018).
31. A. Ndaø, R. Salut, M. Suarez, and F. I. Baida, J. Opt. **20**, 045003 (2018).
32. J. H. Vella, J. H. Goldsmith, A. T. Browning, *et al.*, Phys. Rev. Appl. **5**, 064010 (2016).
33. A. Howes, W. Wang, I. Kravchenko, and J. Valentine, Optica **5**, 787 (2018).
34. M. Khorasaninejad and F. Capasso, Science **358**, eaam8100 (2017).
35. A. Howes, Z. Zhu, D. Curie, *et al.*, Nano Lett. **20**, 4638 (2020). PMID: 32421337.
36. L. Hsu and A. Ndaø, Opt. Lett. **46**, 1293 (2021).
37. J. Parra, J. Navarro-Arenas, M. Menghini, *et al.*, APL Photonics **6**, 121301 (2021).
38. T. Choi, C. Choi, J. Bang, *et al.*, Nano Lett. **24**, 10980 (2024). PMID: 39192436.
39. A. Biegański, M. Perestjuk, R. Armand, *et al.*, Opt. Mater. Express **14**, 862 (2024).
40. R. Petit, ed., *Electromagnetic Theory of Gratings* (Springer, Berlin Heidelberg, 1980).
41. J. Feldmann, N. Youngblood, C. D. Wright, *et al.*, Nat. Commun. **12**, 246 (2021).
42. Z. Cheng, M. Caldarola, C. Li, *et al.*, Opt. Mater. Express **13**, 4707 (2023).
43. M. Kong, H. Lyu, Y. Zhang, *et al.*, ACS Photonics **10**, 3203 (2023).
44. C. Li, T. He, H. Hu, *et al.*, Opt. Mater. Express **14**, 1472 (2024).
45. Q. Zhao, J. Zhou, F. Zhang, and D. Lippens, Mater. Today **12**, 60 (2009).
46. B. A. Slovick, Y. Zhou, Z. G. Yu, *et al.*, Philos. Trans. Royal Soc. A: Math. Phys. Eng. Sci. **375**, 20160072 (2017).

47. C. S. Adams and I. G. Hughes, "159 spatial filtering," in *Optics f2f: From Fourier to Fresnel*, (Oxford University Press, 2018).
48. D. Peri and D. Ritter, *Appl. Opt.* **24**, 1535 (1985).

FULL REFERENCES

- R. W. Wood, "Anomalous diffraction gratings," *Phys. Rev.* **48**, 928–936 (1935).
- S. B. Glybovski, S. A. Tretyakov, P. A. Belov, *et al.*, "Metasurfaces: From microwaves to visible," *Phys. Reports* **634**, 1–72 (2016).
- S. Liu, Z. Ma, J. Pei, *et al.*, "A review of anomalous refractive and reflective metasurfaces," *Nanotechnol. Precis. Eng.* **5**, 025001 (2022).
- B. Rose, T. Rasmussen, and C. Khalfaoui, "Littrow configuration tunable external cavity diode laser with fixed direction output beam," US Patent 6978062B2 (2005). Issued Dec. 20, 2005.
- D. Strickland and G. Mourou, "Compression of amplified chirped optical pulses," *Opt. Commun.* **56**, 219–221 (1985).
- C. J. Hawthorn, K. P. Weber, and R. E. Scholten, "Littrow configuration tunable external cavity diode laser with fixed direction output beam," *Rev. Sci. Instruments* **72**, 4477–4479 (2001).
- M. D. Perry and G. Mourou, "Terawatt to petawatt subpicosecond lasers," *Science* **264**, 917–924 (1994).
- J.-K. Rhee, T. S. Sosnowski, and T. B. Norris, "Chirped-pulse amplification of 85-fs pulses at 250 khz with third-order dispersion compensation by use of holographic transmission gratings," *Opt. Lett.* **19**, 1550–1552 (1994).
- M. S. L. Lee, P. Lalanne, J. C. Rodier, and E. Cambril, "Wide-field-angle behavior of blazed-binary gratings in the resonance domain," *Opt. Lett.* **25**, 1690–1692 (2000).
- P. Lalanne, "Waveguiding in blazed-binary diffractive elements," *J. Opt. Soc. Am. A* **16**, 2517–2520 (1999).
- K. Hehl, J. Bischoff, U. Mohaupt, *et al.*, "High-efficiency dielectric reflection gratings: design, fabrication, and analysis," *Appl. Opt.* **38**, 6257–6271 (1999).
- C. Sauvan, P. Lalanne, and M. S. L. Lee, "Broadband blazing with artificial dielectrics," *Opt. Lett.* **29**, 1593–1595 (2004).
- B. Gralak, S. Enoch, and G. Tayeb, "Anomalous refractive properties of photonic crystals," *J. Opt. Soc. Am. A* **17**, 1012–1020 (2000).
- A. E. Serebryannikov, "One-way diffraction effects in photonic crystal gratings made of isotropic materials," *Phys. Rev. B* **80**, 155117 (2009).
- P. Lalanne, S. Astilean, P. Chavel, *et al.*, "Blazed binary subwavelength gratings with efficiencies larger than those of conventional échelette gratings," *Opt. Lett.* **23**, 1081–1083 (1998).
- Z. Bomzon, V. Kleiner, and E. Hasman, "Pancharatnam–berry phase in space-variant polarization-state manipulations with subwavelength gratings," *Opt. Lett.* **26**, 1424–1426 (2001).
- F. Lu, F. G. Sedgwick, V. Karagodsky, *et al.*, "Planar high-numerical-aperture low-loss focusing reflectors and lenses using subwavelength high contrast gratings," *Opt. Express* **18**, 12606–12614 (2010).
- B. H. Fong, J. S. Colburn, J. J. Ottusch, *et al.*, "Scalar and tensor holographic artificial impedance surfaces," *IEEE Trans. on Antennas Propag.* **58**, 3212–3221 (2010).
- N. Yu, P. Genevet, M. A. Kats, *et al.*, "Light propagation with phase discontinuities: generalized laws of reflection and refraction," *Science* **334**, 333–337 (2011).
- A. Ndao, L. Hsu, J. Ha, *et al.*, "Octave bandwidth photonic fishnet-achromatic-metalens," *Nat. Commun.* **11**, 3205 (2020).
- L. Hsu, M. Dupré, A. Ndao, and B. Kanté, "From parabolic-trough to metasurface-concentrator: assessing focusing in the wave-optics limit," *Opt. Lett.* **42**, 1520–1523 (2017).
- A. Ndao, L. Hsu, W. Cai, *et al.*, "Differentiating and quantifying exosome secretion from a single cell using quasi-bound states in the continuum," *Nanophotonics* **9**, 1081–1086 (2020).
- P. Genevet, F. Capasso, F. Aieta, *et al.*, "Recent advances in planar optics: from plasmonic to dielectric metasurfaces," *Optica* **4**, 139–152 (2017).
- L. Hsu, M. Dupré, A. Ndao, and B. Kanté, "From parabolic-trough to metasurface-concentrator: assessing focusing in the wave-optics limit," *Opt. Lett.* **42**, 1520–1523 (2017).
- G.-Y. Lee, G. Yoon, S.-Y. Lee, *et al.*, "Complete amplitude and phase control of light using broadband holographic metasurfaces," *Nanoscale* **10**, 4237–4245 (2018).
- G. Yang, A. V. Sergienko, and A. Ndao, "Tunable polarization mode conversion using thin-film lithium niobate ridge waveguide," *Opt. Express* **29**, 18565–18571 (2021).
- G. Yang, A. V. Sergienko, and A. Ndao, "Plasmonic loss-mitigating broadband adiabatic polarizing beam splitter," *Opt. Lett.* **47**, 629–632 (2022).
- Y. F. Yu, A. Y. Zhu, R. Paniagua-Domínguez, *et al.*, "High-transmission dielectric metasurface with 2π phase control at visible wavelengths," *Laser & Photonics Rev.* **9**, 412–418 (2015).
- M. I. Shalaev, J. Sun, A. Tsukernik, *et al.*, "High-efficiency all-dielectric metasurfaces for ultracompact beam manipulation in transmission mode," *Nano Lett.* **15**, 6261–6266 (2015).
- J. Ha, A. Ndao, L. Hsu, *et al.*, "Planar dielectric cylindrical lens at 800 nm and the role of fabrication imperfections," *Opt. Express* **26**, 23178–23184 (2018).
- A. Ndao, R. Salut, M. Suarez, and F. I. Baida, "Plasmonless polarization-selective metasurfaces in the visible range," *J. Opt.* **20**, 045003 (2018).
- J. H. Vella, J. H. Goldsmith, A. T. Browning, *et al.*, "Experimental realization of a reflective optical limiter," *Phys. Rev. Appl.* **5**, 064010 (2016).
- A. Howes, W. Wang, I. Kravchenko, and J. Valentine, "Dynamic transmission control based on all-dielectric huygens metasurfaces," *Optica* **5**, 787–792 (2018).
- M. Khorasaninejad and F. Capasso, "Metolenses: Versatile multifunctional photonic components," *Science* **358**, eaam8100 (2017).
- A. Howes, Z. Zhu, D. Curie, *et al.*, "Optical limiting based on huygens' metasurfaces," *Nano Lett.* **20**, 4638–4644 (2020). PMID: 32421337.
- L. Hsu and A. Ndao, "Diffraction-limited broadband optical meta-power-limiter," *Opt. Lett.* **46**, 1293–1296 (2021).
- J. Parra, J. Navarro-Arenas, M. Menghini, *et al.*, "Low-threshold power and tunable integrated optical limiter based on an ultracompact vo2/si waveguide," *APL Photonics* **6**, 121301 (2021).
- T. Choi, C. Choi, J. Bang, *et al.*, "Multiwavelength achromatic deflector in the visible using a single-layer freeform metasurface," *Nano Lett.* **24**, 10980–10986 (2024). PMID: 39192436.
- A. Biegański, M. Perestjuk, R. Armand, *et al.*, "Sb2S3 as a low-loss phase-change material for mid-ir photonics," *Opt. Mater. Express* **14**, 862–870 (2024).
- R. Petit, ed., *Electromagnetic Theory of Gratings* (Springer, Berlin Heidelberg, 1980).
- J. Feldmann, N. Youngblood, C. D. Wright, *et al.*, "Ultra-low-energy programmable non-volatile silicon photonics based on phase-change materials with graphene heaters," *Nat. Commun.* **12**, 246 (2021).
- Z. Cheng, M. Caldarola, C. Li, *et al.*, "Sb2S3 as a low-loss phase-change material for mid-ir photonics," *Opt. Mater. Express* **13**, 4707–4718 (2023).
- M. Kong, H. Lyu, Y. Zhang, *et al.*, "Capping layer effects on Sb2S3-based reconfigurable photonic devices," *ACS Photonics* **10**, 3203–3214 (2023).
- C. Li, T. He, H. Hu, *et al.*, "Low-loss Sb2S3 optical phase shifter enabled by optimizing sputtering conditions," *Opt. Mater. Express* **14**, 1472–1482 (2024).
- Q. Zhao, J. Zhou, F. Zhang, and D. Lippens, "Mie resonance-based dielectric metamaterials," *Mater. Today* **12**, 60–69 (2009).
- B. A. Slovick, Y. Zhou, Z. G. Yu, *et al.*, "Metasurface polarization splitter," *Philos. Trans. Royal Soc. A: Math. Phys. Eng. Sci.* **375**, 20160072 (2017).
- C. S. Adams and I. G. Hughes, "159spatial filtering," in *Optics f2f: From Fourier to Fresnel*, (Oxford University Press, 2018).
- D. Peri and D. Ritter, "Spatial filtering with volume gratings," *Appl. Opt.* **24**, 1535–1540 (1985).